

Ratios of jet and hadron spectra at LHC energies: measuring high- p_T suppression without a pp reference

Jasmine Brewer,¹ Alexander Huss,¹ Aleksas Mazeliauskas,¹ and Wilke van der Schee¹

¹*Theoretical Physics Department, CERN, CH-1211 Geneva 23, Switzerland*

We analyze the reliability of several techniques for computing jet and hadron spectra at different collision energies. This is relevant for discovering energy loss in the upcoming oxygen–oxygen (OO) run at the LHC, for which a reference pp run is currently not planned. For hadrons and jets we compute the ratio of spectra between different pp collision energies in perturbative QCD, which can be used to construct a reference spectrum. Alternatively, it can be interpolated from measured spectra at nearby energies. We estimate the precision of both strategies for the spectra ratio relevant to the oxygen run, and conclude that the central values agree to 4% accuracy for hadrons and 2% accuracy for jets. Finally we propose taking the ratio of OO and pp spectra at different collision energies, which cleanly separates the experimental measurement and theoretical computation.

I. INTRODUCTION

High- p_T hadrons and jets in proton–proton (pp) collisions at the LHC are essential tools for the study of QCD [1]. In heavy-ion collisions, suppression of high momentum hadron and jet spectra is important evidence for the formation of strongly coupled Quark-Gluon Plasma [2–6]. Intense searches for high- p_T hadron or jet spectra suppression in small collision systems, such as proton–lead, have so far been unsuccessful [7–15] despite evidence for collective effects [16–20].

The planned special oxygen–oxygen (OO) run at the LHC in Run 3 [21] offers a unique opportunity to discover high- p_T partonic rescatterings in small collision systems. Several recent model studies indicate that energy loss effects can lead to the suppression of charged hadron spectra up to $\sim 20\%$ for hadrons with momentum ~ 20 GeV [22–25]. The discovery potential therefore relies on the smallness of experimental uncertainties in the measurement and theoretical uncertainties in the reference baseline. In this paper we focus on the latter.

In principle, discovering final-state modification requires differentiating measured spectra for hard probes from the perturbative QCD (pQCD) expectation with nuclear parton distribution functions (nPDFs). However both theoretical and experimental uncertainties on absolute hadron and jet spectra are substantial, so in practice it is crucial to cancel uncertainties by taking the ratio of spectra to a pp reference. However, a measured pp reference at the same energy might not be available in a short OO run [26].

In this work, we study the reliability and accuracy of several methods for measuring jet and hadron suppression in nuclear collisions without a measured pp reference at the same energy. We first consider constructing a pp reference by rescaling a measured spectrum by a theoretically-computed ratio of spectra at different energies. We use the anticipated OO centre-of-mass energy (6.37 TeV) as a timely example [21, 26]. Motivated by Ref. [27] (see also Refs. [28, 29]), we compute these hadron and jet spectra ratios in pQCD and also extract them in a data-driven way from global fits of spectra at

nearby collision energies. Finally, we propose that jet or hadron energy loss can be studied by taking the ratio of OO and pp spectra at *different* collision energies and comparing to the corresponding ratio computed in pQCD. This method disentangles the experimental measurement from theoretical input without significantly inflating the theoretical uncertainties on the baseline compared to the conventional nuclear modification factor.

II. PERTURBATIVE QCD PREDICTIONS

In Fig. 1(a) and Fig. 2(a) we present the ratios between $\sqrt{s} = 6.37$ and 5.02 TeV inclusive hadron and jet spectra in pp collisions computed in pQCD. In collinear QCD factorization, the non-perturbative long distance part of the cross-section—the parton distribution functions (PDFs) and hadron fragmentation functions (FFs)—are factorized at a characteristic scale μ_F from the the hard partonic scattering cross-section. Perturbative cross-sections depend on the unphysical factorization and renormalization scales μ_F and μ_R , which are commonly chosen to represent a typical hard scale of the process. For hadrons we choose the central scales to be the hadron momentum $\mu_0 = p_T^h$, while for jets we used the scalar sum of the transverse momenta of all partons $\mu_0 = \sum_i p_T^i$ [35]. We estimate uncertainties due to missing higher-order corrections by varying μ_F and μ_R around μ_0 by factors of 2 and 1/2 while imposing the restriction $1/2 \leq \mu_F/\mu_R \leq 2$. We vary μ_F for PDFs and FFs independently.

The p_T differential hadron cross-section was computed at leading order (LO) and next-to-leading order (NLO) using a modified version of the INCNLO code [36][37] with LHAPDF grid support [38]. For the charged hadrons we used BKK FFs [39] (the sum of pion and kaon FFs) as the default choice, but we also computed central values using KKP [40] and JAM20 [41] FFs. Jet spectra at LO, NLO, and next-to-next-to-leading order (NNLO) were computed using the NNLOJET framework with the anti- k_T algorithm with a jet radius $R = 0.4$ [42, 43] and using APPLfast interpolation tables [44]. We eval-

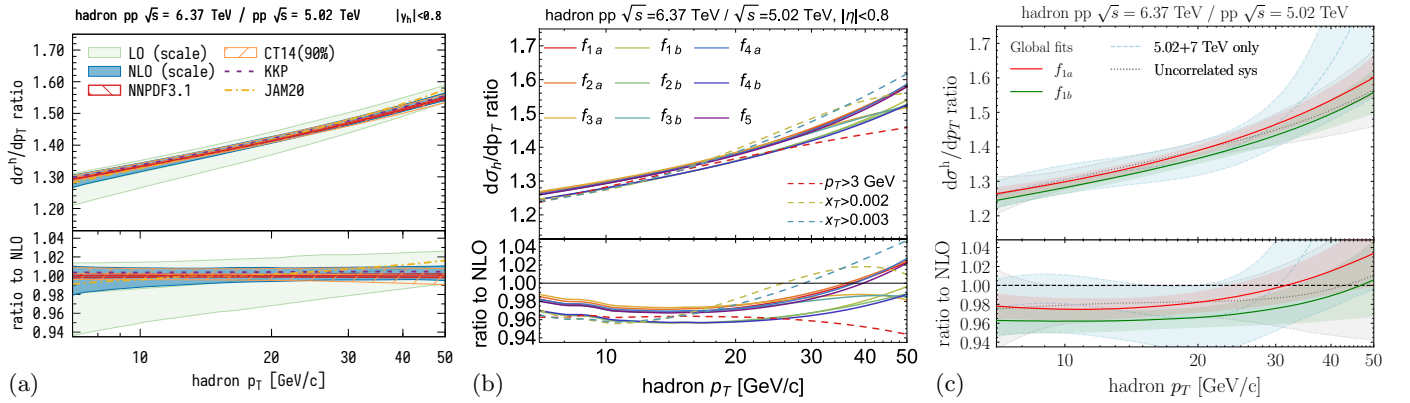


FIG. 1. Ratio of inclusive hadron spectra in pp collisions at $\sqrt{s} = 6.37$ and 5.02 TeV. (a) Ratio from pQCD calculation. Bands show LO (green) and NLO (blue) scale uncertainties and NNPDF3.1 (red) and CT14 (orange) PDF uncertainties. Lines show additional hadron FFs (BKK is the default). (b) Ratio from the best fits using the forms in Table I to ALICE data [30, 31] at 2.76, 5.02 and 7 TeV with $p_T > 7$ GeV (solid) and other p_T cuts for the form f_{1a} (dashed). (c) Ratio from MCMC fits for f_{1a} (red) and f_{1b} (green) with 68% confidence intervals (bands). Fits to only 5.02 and 7 TeV (blue) and using uncorrelated systematic uncertainties (grey) are also shown.

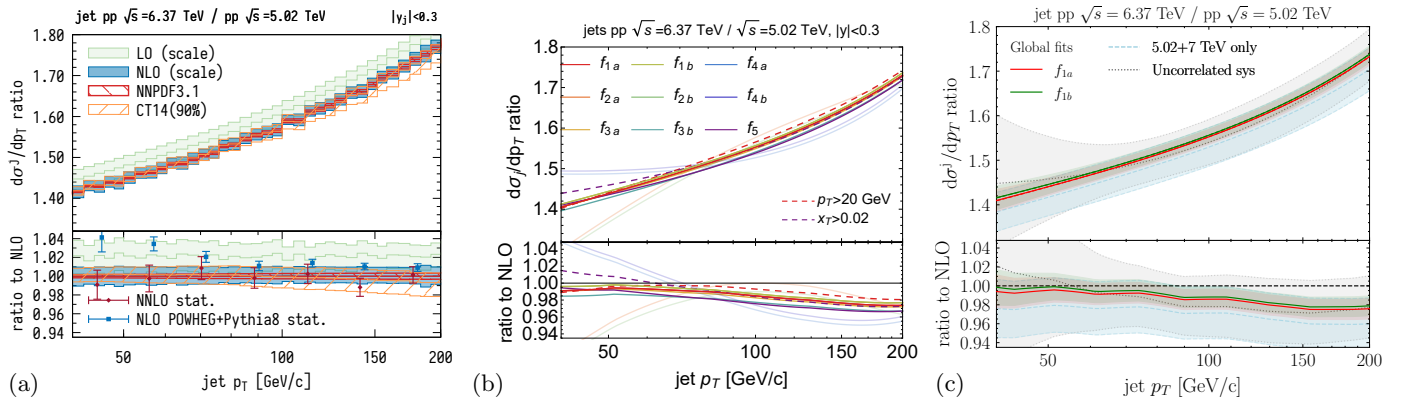


FIG. 2. As in Fig. 1 but for jet spectra. (a) The lower panel includes NNLO partonic and showered NLO results. (b) Solid lines show fits to ATLAS data [32–34] using a standard $p_T > 40$ GeV cut and fit forms with $\chi^2 > 5$ are drawn with lower opacity.

uated uncertainties due to proton PDFs and show for NNPDF3.1 [45] the $\pm 1\sigma$ uncertainty band, while for CT14 [46] we display the 90% confidence level band.

In the lower panel of Fig. 1(a) we see that owing to the cancellation in the correlated scale variation for the ratio between the two energies, the NLO scale envelope for hadrons is less than 2% in the momentum range $p_T^h \in [7, 50]$ GeV and contained within the LO scale band. For jets in Fig. 2(a) the NLO scale envelope is below 1% for $p_T^j \in [40, 200]$ GeV and the central NNLO prediction agrees with it within statistical uncertainties. We also observe excellent cancellation of PDF uncertainties with negligible uncertainties using the NNPDF3.1 set, which are fully consistent with the CT14 error band for both jet and hadron spectra. For hadrons FFs are consistent within 2% accuracy. The showered jet spectra are consistent with the partonic ratio within 2% for $p_T > 60$ GeV. We checked that the deviation at low p_T is due to the \sqrt{s}

dependence of hadronization effects (see below) [34].

We have tested the pQCD computation by direct comparison with existing pp measurements at $\sqrt{s} = 5.02$ and 7 TeV for hadrons by ALICE [30, 31] (Fig. 3) and jets by ATLAS [32, 33] (Fig. 4). The upper panels show the absolute differential spectra, while the lower panels display the ratio to the NLO pQCD prediction (central scale).

The hadron spectra are systematically overpredicted and experimental points are mostly outside the NLO scale band. The large discrepancy in reproducing hadron spectra in hadron collisions is a well known problem of fragmentation functions that are fitted solely to e^+e^- data [47]. Despite the discrepancies in the absolute cross-section, we note that the data to theory ratio with BKK FFs is remarkably stable for $\sqrt{s} = 5.02$ and 7 TeV. To see this we overlay the $\sqrt{s} = 5.02$ TeV ratio to NLO in light grey in the lower panel of Fig. 3(b), which is consistent with the ratio for 7 TeV within experimental uncertainties. Therefore we note that the systematic deviations

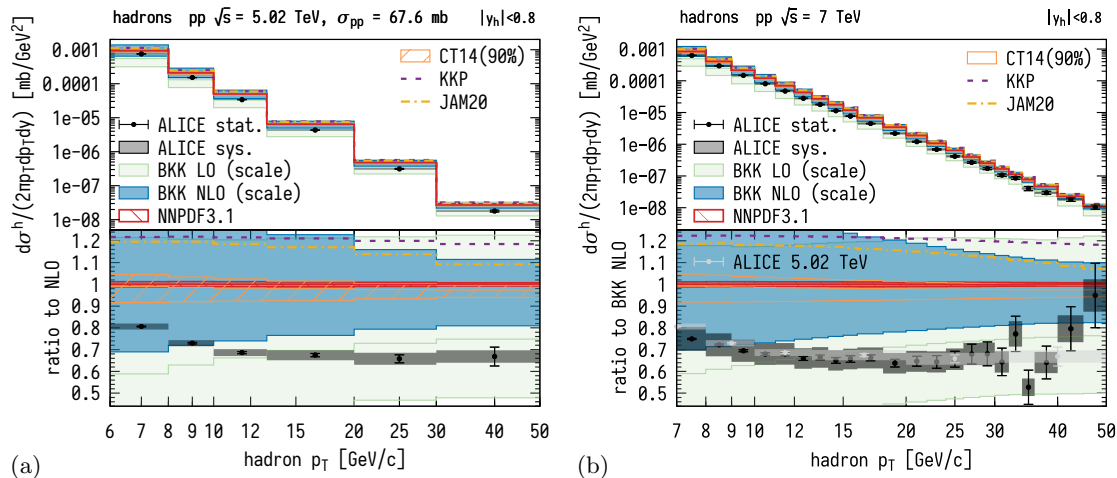


FIG. 3. Differential hadron spectra at (a) 5.02 TeV and (b) 7 TeV by ALICE [30, 31] compared to pQCD predictions. Absolute spectra (upper panels) and ratio to NLO (lower panels) are shown. Scale uncertainties are shown by solid bands, PDF uncertainty by patterned bands, and additional FFs by lines (BKK is the default). The ratio of 5.02 TeV data to NLO is overlaid in light grey in the lower panel of (b).

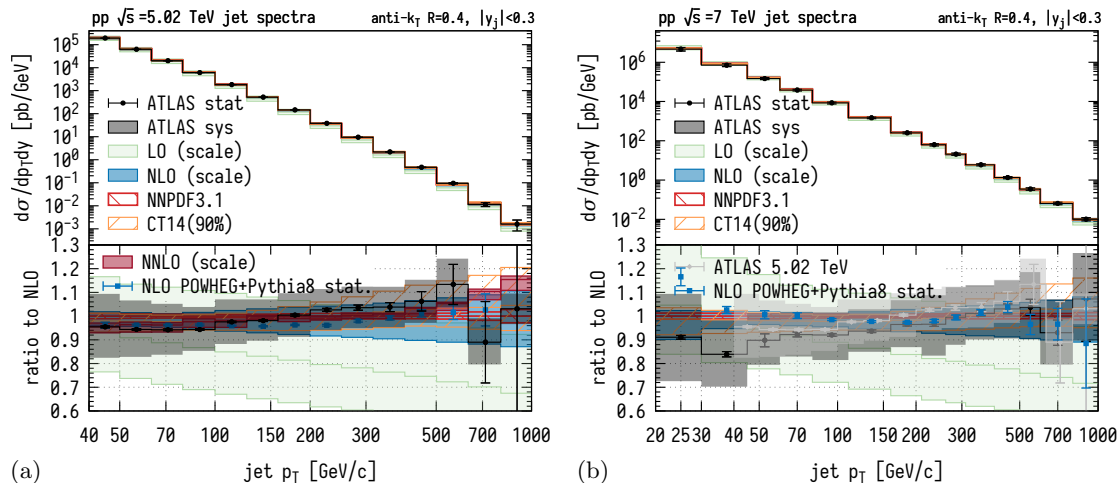


FIG. 4. Differential jet spectra at (a) 5.02 TeV and (b) 7 TeV by ATLAS [32, 33] compared to pQCD predictions. Absolute spectra (upper panels) and ratio to NLO (lower panels) are shown. Scale uncertainties are shown by solid bands and PDF uncertainty by patterned bands. NNLO scale band and showered NLO results are shown in the lower panel of (a). The ratio of 5.02 TeV data to NLO is overlaid in light grey in the lower panel of (b).

largely cancel between two energies and pQCD predicts a 5.02/7 TeV ratio that is consistent with data.

The jet spectrum at 5.02 TeV in Fig. 4(a) is reproduced within NLO scale uncertainties with a slightly rising data to theory ratio that is captured by NNLO corrections. The non-perturbative and showering effects of jet spectra were tested at NLO using POWHEG+Pythia8 [48, 49][50] and were found to be consistent with fixed-order NLO predictions within scale uncertainties. Fig. 4(b) shows a similar plot for 7 TeV data (with 5.02 TeV overlaid in light grey). Again we see that the data to NLO ratio changes little between the two energies and the showered spectra at NLO are consistent with data down to

40 GeV. This was also seen in the ATLAS analysis of jets at 2.76 and 7 TeV [34].

III. INTERPOLATION OF EXPERIMENTAL DATA

Here we obtain the ratios of inclusive hadron and jet spectra in pp collisions at $\sqrt{s} = 6.37$ and 5.02 TeV from interpolation of measured data at nearby collision energies. Interpolation was used to construct references for 5.02 TeV proton-lead run [8, 10, 11, 51, 52] (see also [28, 29] and [53]). A first look at the interpolated hadron

spectra ratio for oxygen was reported in a recent ALICE public note [27]. Here we present a detailed study of the uncertainties arising from interpolation, both by studying the dependence on the functional form of the fits (Fig. 1(b) and Fig. 2(b)) and using Markov Chain Monte Carlo (MCMC) fits to propagate data uncertainties into uncertainties on the spectra ratio (Fig. 1(c) and Fig. 2(c)).

To demonstrate the feasibility of these techniques we will use existing experimental data from LHC Run 1 and 2 at $\sqrt{s} = 2.76, 5.02, \text{ and } 7 \text{ TeV}$. This is only illustrative, since pp references taken during Run 3 will be at different energies (e.g., 5.02, 8.8, and 13.6 TeV) [21]. For charged hadrons we use differential cross-sections with $|\eta| < 0.8$ measured by ALICE [30, 31]. At $\sqrt{s} = 2.76$ and 5.02 TeV we convert measured spectra to cross-sections using inelastic hadronic cross-sections of 61.8 and 67.6 mb, respectively [54]. We use ATLAS measurements of inclusive jet spectra with $|y| < 0.3$ and anti- k_T radius $R = 0.4$ [32–34]. Unless otherwise stated, we fit only data satisfying $p_T > 7 \text{ GeV}$ for hadrons and $p_T > 40 \text{ GeV}$ for jets. In the appendix A, we also show results for CMS measurements of hadron spectra at the same energies [7, 55, 56].

We obtain the best fits by maximizing the log likelihood function (or minimizing $\chi^2 \equiv -2 \log \mathcal{L}$), with

$$\log \mathcal{L} = -\frac{1}{2} \sum_{\sqrt{s}, i, j} \Delta y_i^{\sqrt{s}} (C^{\sqrt{s}})_{ij}^{-1} \Delta y_j^{\sqrt{s}}, \quad (1)$$

$$\Delta y_i^{\sqrt{s}} = y_i^{\sqrt{s}} - \int_{\text{bin } i} dp_T f(\sqrt{s}, p_T). \quad (2)$$

Here $y_i^{\sqrt{s}}$ is the i -th datapoint at \sqrt{s} , $f(\sqrt{s}, p_T)$ is a fit to the differential spectrum, and $C^{\sqrt{s}}$ is the covariance matrix for that collision energy. In the absence of the available covariance matrix of experiment uncertainties, we model $C^{\sqrt{s}}$ with two limiting cases. We treat $C^{\sqrt{s}}$ as a sum of uncorrelated uncertainties $\sigma_{\text{uncorr}}^{\sqrt{s}}$ and a luminosity uncertainty $\sigma_{\text{lum}}^{\sqrt{s}}$ that is fully correlated at each energy,

$$(C^{\sqrt{s}})_{ij} = (\sigma_{\text{uncorr}, i}^{\sqrt{s}})^2 \delta_{ij} + (\sigma_{\text{lum}}^{\sqrt{s}})^2. \quad (3)$$

In the first case, we consider that all systematic uncertainties apart from the luminosity uncertainty cancel in the ratio between energies, so the uncorrelated uncertainty is only statistical. For comparison we also consider the opposite limit that all non-luminosity systematic uncertainties are fully uncorrelated and add them in quadrature to the statistical uncertainties. We expect that these two scenarios bracket the actual covariance matrix of experimental uncertainties, which, we hope, will be provided with future measurements.

The high- p_T differential cross-section of hadrons or jets can be approximated by a power of \sqrt{s} times a function of the dimensionless variable $x_T = 2p_T/\sqrt{s}$ [57–59]. We therefore perform global fits of either hadron or jet spec-

tra using one of nine fitting formulas of the form

$$\frac{d\sigma}{dp_T} = f(\sqrt{s}, p_T) = A\sqrt{s}^\beta \hat{x}_T^{n(\hat{x}_T, \sqrt{s})}. \quad (4)$$

Here A is a dimensionful normalization constant, $\sqrt{s} \equiv \sqrt{s}/2.76 \text{ TeV}$ and $\hat{x}_T \equiv x_T/x_0$, with $x_0 = 0.003$ ($x_0 = 0.02$) for hadrons (jets). We summarize different parametrizations in Table I. The first eight forms come in pairs, with the only difference being the \sqrt{s} dependence of the coefficients in the exponent $n(\hat{x}_T, \sqrt{s})$, which we assume to be either linear in \sqrt{s} or in $\log \sqrt{s}$. The form f_2 differs from f_1 in using a power of x_T instead of \hat{x}_T . Restricted to 2.76 and 7 TeV data, the f_{2b} fit is equivalent to the method used in [11, 34]. We calculate the reduced $\chi_\nu^2 = \chi^2/(N-p)$ for each fit form in Table I, with N and p the number of data points and parameters. For default p_T cuts, $N = 32$ for hadrons and 37 for jets. Our preferred fit forms $f_{1a,1b}$ with eight independent parameters have $\chi_\nu^2 \approx 0.75$ and 1.1 for hadrons and jets respectively, indicating a good quality of fits. For jet spectra using x_T instead of \hat{x}_T as in $f_{2a,2b}$, or reducing the number of fit parameters to 6 as in $f_{4a,4b}$ considerably worsens the fit quality. Increasing fit parameters to 10 in $f_{3a,3b}$ or considering mixed \sqrt{s} dependence in f_5 left χ_ν^2 for jets essentially unchanged. For hadrons all nine fit forms give comparable fit quality.

We use the interpolation functions to compute the jet and hadron spectra ratios at $\sqrt{s} = 6.37$ and 5.02 TeV shown in Figs. 1(b) and 2(b). For hadrons the fit forms with linear \sqrt{s} dependence result in about 2% larger ratio compared to $\log \sqrt{s}$. For jets there is no strong dependence on the \sqrt{s} parametrization. For jets fit forms $f_{2a,2b,4a,4b}$ did not lead to a satisfactory χ_ν^2 and are hence drawn at lower opacity in the figure.

We also investigate our fit sensitivity to data selection using the f_{1a} fit form in Figs. 1(b) and 2(b). The lower p_T (or x_T) cut on data is necessary for hadrons, which are measured to much lower p_T than x_T scaling applies. For hadrons we consider $x_T > 0.003$ ($\chi_\nu^2 = 1.14$), $p_T > 3 \text{ GeV}$ ($\chi_\nu^2 = 1.72$), and $x_T > 0.002$ ($\chi_\nu^2 = 1.60$). For the latter two, the fit is not consistent with the data if all systematics cancel ($\chi_\nu^2 = 16.2$ and $\chi_\nu^2 = 8.7$) so we include 1% uncorrelated systematic uncertainties in these fits. Lowering the p_T cut to 3 GeV changes the hadron ratio at higher momentum, but with worse χ_ν^2 . For jets we show results for $p_T > 20 \text{ GeV}$ (all available data) and $x_T > 0.02$ with $\chi_\nu^2 = 3.36$ and 1.16. Jet fits are relatively insensitive to the data selection.

Next we study the propagation of experimental uncertainties to the interpolated ratio. We use $f_{1a,1b}$ (again with $p_T > 7 \text{ GeV}$ for hadrons and $p_T > 40 \text{ GeV}$ for jets) and perform MCMC global fits using the emcee implementation [60]. We use the likelihood function Eq. (1) to sample the distribution of parameters consistent with the data at the anchor energies given their uncertainty covariance matrix (from Eq. (3)). In particular, we initialize a chain of 200 walkers with a Gaussian distribution

TABLE I. Fitting forms together with the resulting reduced χ^2 for fits of hadron ($p_T > 7$ GeV) and jet ($p_T > 40$ GeV) spectra for pp collisions at $\sqrt{s} = 2.76, 5.02$ and 7 TeV. Here $\hat{x}_T = x_T/x_0$ with $x_0 = 0.003$ for hadrons and $x_0 = 0.02$ for jets. a, b, c and d are linear functions of either $\sqrt{\hat{s}} \equiv \sqrt{s}/2.76$ TeV or $\log \sqrt{\hat{s}}$, e.g. $a(\hat{s}) = a_0 + a_1\sqrt{\hat{s}}$ or $a(\hat{s}) = a_0 + a_1 \log \sqrt{\hat{s}}$. All other variables are fit parameters.

function	fit form	\sqrt{s} dep.	p	χ^2_{ν} -hadrons	χ^2_{ν} -jets
f_{1a}	$A \left(\sqrt{\hat{s}} \right)^\beta \hat{x}_T^{a(\hat{s})+b(\hat{s})\hat{x}_T+c(\hat{s}) \log \hat{x}_T}$	linear	8	0.75	1.11
f_{1b}	$A \left(\sqrt{\hat{s}} \right)^\beta \hat{x}_T^{a(\hat{s})+b(\hat{s})\hat{x}_T+c(\hat{s}) \log \hat{x}_T}$	log linear	8	0.75	1.15
f_{2a}	$A \left(\sqrt{\hat{s}} \right)^\beta x_T^{a(\hat{s})+b(\hat{s})x_T+c(\hat{s}) \log x_T}$	linear	8	0.75	5.02
f_{2b}	$A \left(\sqrt{\hat{s}} \right)^\beta x_T^{a(\hat{s})+b(\hat{s})x_T+c(\hat{s}) \log x_T}$	log linear	8	0.75	5.10
f_{3a}	$A \left(\sqrt{\hat{s}} \right)^\beta \hat{x}_T^{a(\hat{s})+b(\hat{s})\hat{x}_T+c(\hat{s}) \log \hat{x}_T+d(\hat{s})\hat{x}_T / \log \hat{x}_T}$	linear	10	0.80	1.19
f_{3b}	$A \left(\sqrt{\hat{s}} \right)^\beta \hat{x}_T^{a(\hat{s})+b(\hat{s})\hat{x}_T+c(\hat{s}) \log \hat{x}_T+d(\hat{s})\hat{x}_T / \log \hat{x}_T}$	log linear	10	0.80	1.18
f_{4a}	$A \left(\sqrt{\hat{s}} \right)^\beta \hat{x}_T^{a(\hat{s})+b(\hat{s})\hat{x}_T}$	linear	6	0.70	5.05
f_{4b}	$A \left(\sqrt{\hat{s}} \right)^\beta \hat{x}_T^{a(\hat{s})+b(\hat{s})\hat{x}_T}$	log linear	6	0.70	5.10
f_5	$A \left(\sqrt{\hat{s}} \right)^\beta \hat{x}_T^{a_0+a_1\sqrt{\hat{s}}+a_2\hat{x}_T+a_3 \log(\sqrt{\hat{s}})+a_4 \log(\hat{x}_T)}$	—	7	0.73	1.10

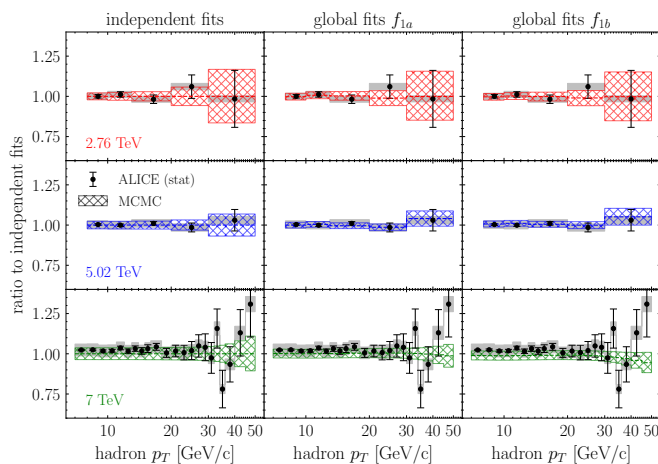


FIG. 5. Fits to ALICE hadron spectra at $\sqrt{s} = 2.76, 5.02,$ and 7 TeV [32, 33], anchoring the interpolation for the results in Fig. 1c. The left panel shows independent fits to the spectrum at each energy normalized to the median value of the independent fit at that energy. The center and right panels show results for global fits f_{1a} and f_{1b} normalized to the median value of the independent fit at that energy. Uncorrelated (statistical) uncertainties are shown in bars and luminosity uncertainties are grey boxes. Hatched bands indicate the 68% confidence interval of the MCMC fits.

in the parameter space around the maximum likelihood point. The walkers are evolved according to the likelihood function Eq. (1) for 10^4 steps with no constraints in the parameter space, i.e., with uniform priors. We use only the last 2000 steps for the computation of the confidence intervals. Crucially, this method produces a distribution of fits obeying the likelihood function with experimental uncertainties, rather than a single fit that maximizes the likelihood. We then compute the 68% confidence intervals on the interpolated ratio around the median value from the distribution of fit values in each momentum bin.

Figs. 1(c) and 2(c) show the median and the 68% confidence bands for the 6.37/5.02 TeV spectra ratios for

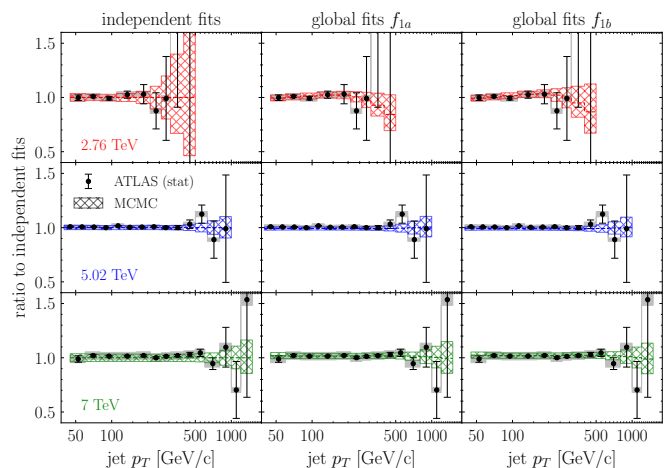


FIG. 6. Fits to ATLAS jet spectra at $\sqrt{s} = 2.76, 5.02,$ and 7 TeV [32–34], anchoring the interpolation for the results in Fig. 2c. The left panel shows independent fits to the spectrum at each energy normalized to the median value of the independent fit at that energy. The center and right panels show results for global fits f_{1a} and f_{1b} normalized to the median value of the independent fit at that energy. Uncorrelated (statistical) uncertainties are shown in bars and luminosity uncertainties are grey boxes. Hatched bands indicate the 68% confidence interval of the MCMC fits.

hadrons and jets. For hadrons, statistical and luminosity uncertainties on the spectra at the anchor energies give rise to few-percent uncertainties for $p_T \lesssim 30$ GeV that grow to $\sim 5\%$ at 50 GeV. f_{1a} and f_{1b} are consistent within uncertainty bands but shifted from each other at the 2% level. Both fit forms deviate from the NLO pQCD prediction by a few percent for $p_T \lesssim 20$ GeV. For jets the results for f_{1a} and f_{1b} are very similar with $\sim 2\%$ uncertainties for all p_T shown. The interpolated ratio has up to 2% deviations from NLO pQCD for $p_T \gtrsim 120$ GeV. For both hadrons and jets, fits using only 5.02 and 7 TeV data have much larger uncertainties than fits of three energies. If non-luminosity systematic uncertainties are uncorrelated and not cancelled in the ratio, the median

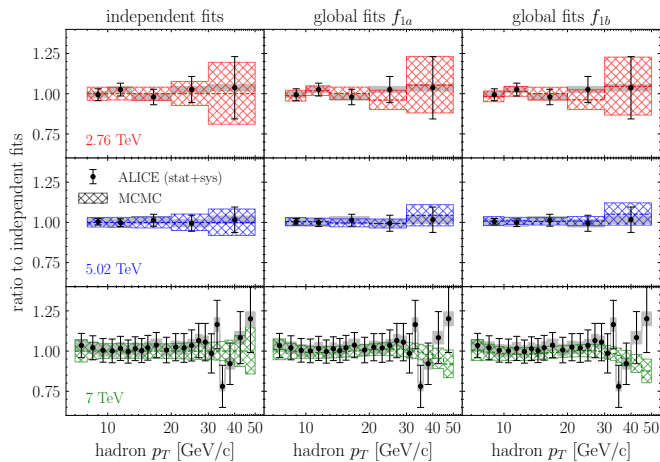


FIG. 7. Same as Fig. 5, but assuming uncorrelated systematic uncertainties. Uncorrelated (statistical + systematic) uncertainties are shown in bars and luminosity uncertainties are grey boxes.

6.37/5.02 TeV ratio is similar but with a significant increase in uncertainties. In the appendix A we show the same analysis for CMS hadron data, which has milder p_T dependence of the ratio but is consistent within uncertainties.

We test the MCMC global fits by showing the extracted confidence intervals compared to measured spectra at the anchor energies. We benchmark the global fits against fits to the individual spectra using the forms f_1 at a single center-of-mass energy (taking $a_1 = 0$ in Table I), in which case $f_{1a} = f_{1b}$. We show the independent fits (left panel) and global fits f_{1a} and f_{1b} (center and right panels, respectively) for hadrons (Fig. 5) and for jets (Fig. 6), assuming that systematic uncertainties besides the luminosity uncertainty cancel fully between energies. For visual clarity we show both data and fits as a ratio to the central value of the independent fit. Figs. 7 and 8 show the same information except assuming that non-luminosity systematic uncertainties are fully uncorrelated. We note that in Figs. 7 and 8 the MCMC bands for the independent fits do not encompass the uncertainties (particularly obvious at 7 TeV in Fig. 7 and 5.02 TeV in Fig. 8), suggesting that the all systematic uncertainties cannot be considered fully uncorrelated between neighboring p_T bins.

IV. MIXED-ENERGY NUCLEAR MODIFICATION FACTOR

For the standard nuclear modification factor, the theoretical no-energy-loss baseline differs from unity due to nuclear PDFs [61], so it is necessary to compare measurements to theoretical calculations to establish the presence of (small) final-state effects [22]. In this section we propose that energy loss in OO collisions could be discovered by measuring the ratio of jet or hadron spectra in OO to

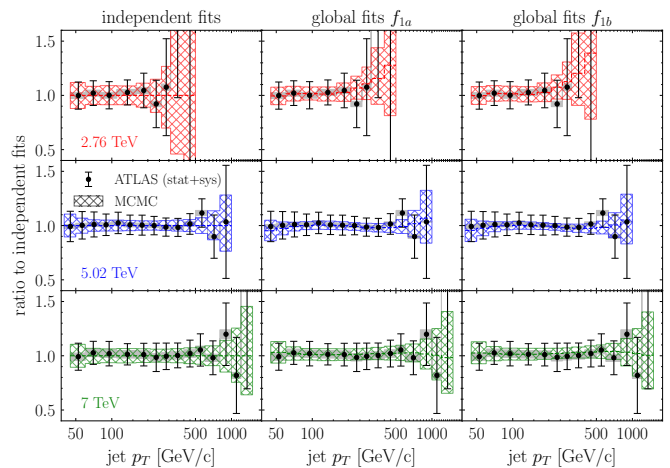


FIG. 8. Same as Fig. 6, but assuming uncorrelated systematic uncertainties. Uncorrelated (statistical + systematic) uncertainties are shown in bars and luminosity uncertainties are grey boxes.

pp spectra at a different nearby energy, and comparing this to the nPDF baseline in the absence of energy loss. In Fig. 9 we show the pQCD baseline for the ratios of hadron and jet cross-sections in minimum bias OO collisions at 6.37 TeV (per nucleon-nucleon pair) divided by spectra in pp collisions at 5.02 TeV.

We show nPDF uncertainties for EPPS16 [62], nNNPDF2.0 [63] and the recent nCTEQ15(WZSIH) version [64]. EPPS16 and nCTEQ15 are consistent within the larger EPPS16 uncertainties. nNNPDF2.0 exhibits a systematic downward shift for hadrons and jets with $p_T < 100$ GeV. New nCTEQ15 nPDFs including inclusive hadron production and LHC W/Z data have very stringent error bands (below 3% for hadrons and 2% for jets). It will be important to compare predictions from the upcoming iterations of EPPS21 and nNNPDF3.0 global fits with extended datasets. Since nPDF global fits do not contain data with oxygen nuclei and hadronic data is only available for heavy or very light nuclei, interpolated nPDFs for oxygen nuclei are potentially sensitive to the assumed A dependence of nPDFs. Complementary pO data would be very valuable in validating and constraining nPDF uncertainties in light nuclei [65].

V. DISCUSSION

In this work, we have predicted the ratio of hadron and jet spectra at two collision energies (6.37 and 5.02 TeV) in pp collisions, which can be used to construct the reference spectrum for the upcoming OO run at the LHC. We used pQCD calculations and data-driven interpolation and estimated theoretical uncertainties of both methods. The residual pQCD uncertainty on the ratio is below 2% for hadrons and below 2% for jets above 60 GeV. The uncertainty from the data-driven interpolation can be as low

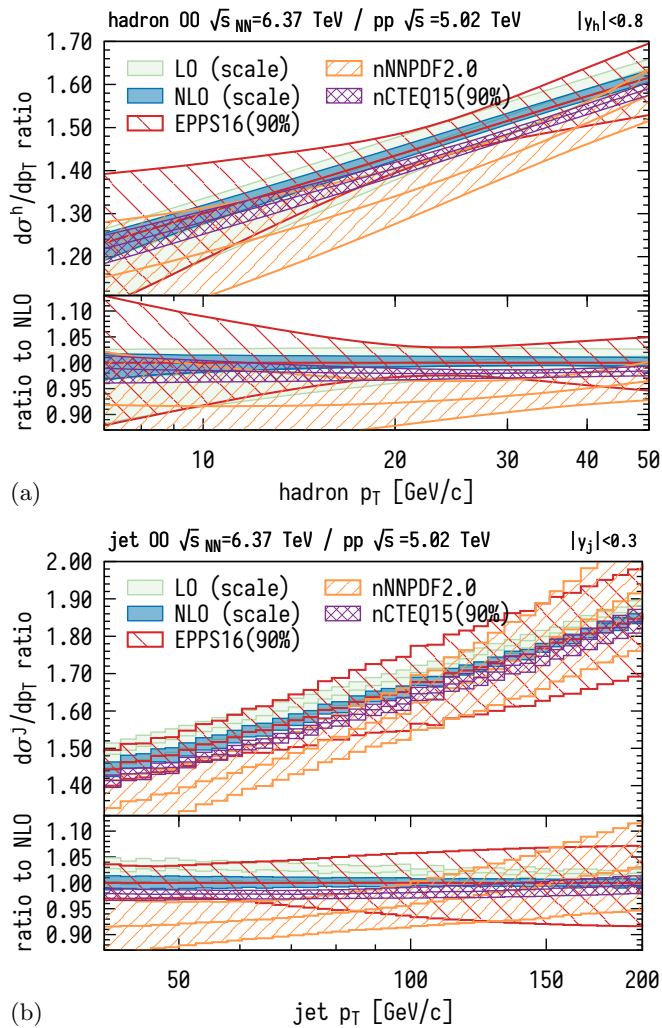


FIG. 9. No-energy-loss baseline for the ratio of hadron (a) and jet (b) spectra in OO collisions at $\sqrt{s_{NN}} = 6.37$ TeV with that in pp at $\sqrt{s} = 5.02$ TeV. Scale uncertainties (solid green and blue) and nPDF uncertainties (pattern) are shown.

as 3%, but is sensitive to the selection of data in the fits

and relies on using three energies with significant cancellation of systematic uncertainties. It would be necessary to perform the interpolation analysis with the LHC Run 3 data at the actual collision energies once it becomes available. If both methods are considered together, the central values of pQCD and interpolated ratios deviate from each other by up to 4% for hadrons and 2% for jets.

Alternatively, we propose that the measured jet or hadron spectra in 6.37 TeV OO collisions can be compared to the spectra in pp collisions at a different energy by forming a mixed-energy nuclear modification ratio. In this case, there is no need to construct a pp reference spectrum and the measured ratio can be compared directly to the pQCD baseline computation. The mixed-energy ratios have few percent scale uncertainties similar to the mixed-energy pp ratios from pQCD. Nevertheless, these uncertainties are smaller or comparable to nPDF uncertainties and smaller than uncertainties we estimate for interpolating a reference from measured data. We note that the mixed-energy nPDF baseline relies on the center-of-mass energy dependence of pQCD being correct, which can be cross-checked with data. Different nPDFs have significant differences in their uncertainty bands, but the newest nCTEQ15 version has uncertainties reduced to a few percent. Measurements in pO collisions will be especially important for providing direct constraints on the nPDFs of oxygen [65]. Since a pp reference measurement is not planned at the pO energy in the LHC Run 3, reference interpolation and mixed-energy ratios may also be relevant for global nPDF fits.

The computer code to perform the MCMC fits is based on [66] and is publicly available at <https://github.com/jasminebrewer/spectra-from-MCMC>.

VI. ACKNOWLEDGEMENTS

We thank Pit Duwentäster for nCTEQ15 nPDFs and gratefully acknowledge valuable discussions with Andrea Dainese, Silvia Ferrario Ravasio, Alexander Kalweit, Yen-Jie Lee, Pier Monni, Petja Paakkinen, Anne Sickles, Jesse Thaler, Marta Verweij, Vytautas Vislavicius, and Urs Wiedemann.

-
- [1] J. M. Butterworth, G. Dissertori, and G. P. Salam, *Ann. Rev. Nucl. Part. Sci.* **62**, 387 (2012), arXiv:1202.0583 [hep-ex].
 - [2] J. Adams *et al.* (STAR), *Nucl. Phys. A* **757**, 102 (2005), arXiv:nucl-ex/0501009.
 - [3] K. Adcox *et al.* (PHENIX), *Nucl. Phys. A* **757**, 184 (2005), arXiv:nucl-ex/0410003.
 - [4] G. Aad *et al.* (ATLAS), *Phys. Rev. Lett.* **105**, 252303 (2010), arXiv:1011.6182 [hep-ex].
 - [5] S. Chatrchyan *et al.* (CMS), *Phys. Rev.* **C84**, 024906 (2011), arXiv:1102.1957 [nucl-ex].
 - [6] K. Aamodt *et al.* (ALICE), *Phys. Lett. B* **696**, 30 (2011), arXiv:1012.1004 [nucl-ex].
 - [7] V. Khachatryan *et al.* (CMS), *JHEP* **04**, 039 (2017), arXiv:1611.01664 [nucl-ex].
 - [8] V. Khachatryan *et al.* (CMS), *Eur. Phys. J. C* **76**, 372 (2016), arXiv:1601.02001 [nucl-ex].
 - [9] S. Acharya *et al.* (ALICE), *JHEP* **11**, 013 (2018), arXiv:1802.09145 [nucl-ex].
 - [10] G. Aad *et al.* (ATLAS), *Phys. Lett. B* **763**, 313 (2016), arXiv:1605.06436 [hep-ex].
 - [11] G. Aad *et al.* (ATLAS), *Phys. Lett. B* **748**, 392 (2015), arXiv:1412.4092 [hep-ex].

- [12] C. Aidala *et al.* (PHENIX), *Phys. Rev. C* **101**, 034910 (2020), [arXiv:1906.09928 \[hep-ex\]](#).
- [13] A. Adare *et al.* (PHENIX), *Phys. Rev. Lett.* **116**, 122301 (2016), [arXiv:1509.04657 \[nucl-ex\]](#).
- [14] S. Acharya *et al.* (ALICE), *Phys. Lett. B* **783**, 95 (2018), [arXiv:1712.05603 \[nucl-ex\]](#).
- [15] J. Adam *et al.* (ALICE), *Phys. Rev. C* **91**, 064905 (2015), [arXiv:1412.6828 \[nucl-ex\]](#).
- [16] S. Chatrchyan *et al.* (CMS), *Phys. Lett. B* **718**, 795 (2013), [arXiv:1210.5482 \[nucl-ex\]](#).
- [17] G. Aad *et al.* (ATLAS), *Phys. Rev. Lett.* **110**, 182302 (2013), [arXiv:1212.5198 \[hep-ex\]](#).
- [18] B. Abelev *et al.* (ALICE), *Phys. Lett. B* **719**, 29 (2013), [arXiv:1212.2001 \[nucl-ex\]](#).
- [19] J. Adam *et al.* (ALICE), *Nature Phys.* **13**, 535 (2017), [arXiv:1606.07424 \[nucl-ex\]](#).
- [20] R. Aaij *et al.* (LHCb), *Phys. Lett. B* **762**, 473 (2016), [arXiv:1512.00439 \[nucl-ex\]](#).
- [21] Z. Citron *et al.*, *CERN Yellow Rep. Monogr.* **7**, 1159 (2019), [arXiv:1812.06772 \[hep-ph\]](#).
- [22] A. Huss, A. Kurkela, A. Mazeliauskas, R. Paatelainen, W. van der Schee, and U. A. Wiedemann, *Phys. Rev. Lett.* **126**, 192301 (2021), [arXiv:2007.13754 \[hep-ph\]](#).
- [23] A. Huss, A. Kurkela, A. Mazeliauskas, R. Paatelainen, W. van der Schee, and U. A. Wiedemann, *Phys. Rev. C* **103**, 054903 (2021), [arXiv:2007.13758 \[hep-ph\]](#).
- [24] B. G. Zakharov, *JHEP* **09**, 087 (2021), [arXiv:2105.09350 \[hep-ph\]](#).
- [25] Y.-F. Liu, W.-J. Xing, X.-Y. Wu, G.-Y. Qin, S. Cao, and H. Xing, (2021), [arXiv:2107.01522 \[hep-ph\]](#).
- [26] J. Brewer, A. Mazeliauskas, and W. van der Schee, in *Opportunities of OO and pO collisions at the LHC* (2021) [arXiv:2103.01939 \[hep-ph\]](#).
- [27] S. Acharya *et al.* (ALICE), *ALICE-PUBLIC-2021-004* (2021).
- [28] D. G. d'Enterria, *J. Phys. G* **31**, S491 (2005), [arXiv:nucl-ex/0411049](#).
- [29] F. Arleo, D. d'Enterria, and A. S. Yoon, *JHEP* **06**, 035 (2010), [arXiv:1003.2963 \[hep-ph\]](#).
- [30] S. Acharya *et al.* (ALICE), *JHEP* **11**, 013 (2018), [arXiv:1802.09145 \[nucl-ex\]](#).
- [31] B. B. Abelev *et al.* (ALICE), *Eur. Phys. J. C* **73**, 2662 (2013), [arXiv:1307.1093 \[nucl-ex\]](#).
- [32] G. Aad *et al.* (ATLAS), *Phys. Rev. D* **86**, 014022 (2012), [arXiv:1112.6297 \[hep-ex\]](#).
- [33] M. Aaboud *et al.* (ATLAS), *Phys. Lett. B* **790**, 108 (2019), [arXiv:1805.05635 \[nucl-ex\]](#).
- [34] G. Aad *et al.* (ATLAS), *Eur. Phys. J. C* **73**, 2509 (2013), [arXiv:1304.4739 \[hep-ex\]](#).
- [35] J. Currie, A. Gehrman-De Ridder, T. Gehrman, E. W. N. Glover, A. Huss, and J. a. Pires, *JHEP* **10**, 155 (2018), [arXiv:1807.03692 \[hep-ph\]](#).
- [36] F. Aversa, P. Chiappetta, M. Greco, and J. P. Guillet, *Nucl. Phys. B* **327**, 105 (1989).
- [37] http://laphth.cnrs.fr/PHOX_FAMILY/readme_inc.html.
- [38] A. Buckley, J. Ferrando, S. Lloyd, K. Nordström, B. Page, M. Rüfenacht, M. Schönherr, and G. Watt, *Eur. Phys. J. C* **75**, 132 (2015), [arXiv:1412.7420 \[hep-ph\]](#).
- [39] J. Binnewies, B. A. Kniehl, and G. Kramer, *Z. Phys. C* **65**, 471 (1995), [arXiv:hep-ph/9407347](#).
- [40] B. A. Kniehl, G. Kramer, and B. Potter, *Nucl. Phys. B* **582**, 514 (2000), [arXiv:hep-ph/0010289](#).
- [41] E. Moffat, W. Melnitchouk, T. Rogers, and N. Sato, (2021), [arXiv:2101.04664 \[hep-ph\]](#).
- [42] J. Currie, E. W. N. Glover, and J. Pires, *Phys. Rev. Lett.* **118**, 072002 (2017), [arXiv:1611.01460 \[hep-ph\]](#).
- [43] T. Gehrman *et al.*, *PoS RADCOR2017*, 074 (2018), [arXiv:1801.06415 \[hep-ph\]](#).
- [44] D. Britzger *et al.*, *Eur. Phys. J. C* **79**, 845 (2019), [arXiv:1906.05303 \[hep-ph\]](#).
- [45] R. D. Ball *et al.* (NNPDF), *Eur. Phys. J. C* **77**, 663 (2017), [arXiv:1706.00428 \[hep-ph\]](#).
- [46] S. Dulat, T.-J. Hou, J. Gao, M. Guzzi, J. Huston, P. Nadolsky, J. Pumplin, C. Schmidt, D. Stump, and C. P. Yuan, *Phys. Rev. D* **93**, 033006 (2016), [arXiv:1506.07443 \[hep-ph\]](#).
- [47] D. d'Enterria, K. J. Eskola, I. Helenius, and H. Paukkunen, *Nucl. Phys. B* **883**, 615 (2014), [arXiv:1311.1415 \[hep-ph\]](#).
- [48] S. Alioli, P. Nason, C. Oleari, and E. Re, *JHEP* **06**, 043 (2010), [arXiv:1002.2581 \[hep-ph\]](#).
- [49] T. Sjöstrand, S. Ask, J. R. Christiansen, R. Corke, N. Desai, P. Ilten, S. Mrenna, S. Prestel, C. O. Rasmussen, and P. Z. Skands, *Comput. Phys. Commun.* **191**, 159 (2015), [arXiv:1410.3012 \[hep-ph\]](#).
- [50] POWHEG Events were generated using the jet p_T of the underlying Born kinematics as the central scale (default) and the settings `bornzerodamp=1` and `hdamp=100`.
- [51] B. Abelev *et al.* (ALICE), *Phys. Rev. Lett.* **110**, 082302 (2013), [arXiv:1210.4520 \[nucl-ex\]](#).
- [52] V. Khachatryan *et al.* (CMS), *Eur. Phys. J. C* **75**, 237 (2015), [arXiv:1502.05387 \[nucl-ex\]](#).
- [53] V. M. Abazov *et al.* (D0, TOTEM), (2020), [arXiv:2012.03981 \[hep-ex\]](#).
- [54] C. Loizides, J. Kamin, and D. d'Enterria, *Phys. Rev. C* **97**, 054910 (2018), [Erratum: *Phys.Rev.C* **99**, 019901 (2019)], [arXiv:1710.07098 \[nucl-ex\]](#).
- [55] S. Chatrchyan *et al.* (CMS), *JHEP* **08**, 086 (2011), [arXiv:1104.3547 \[hep-ex\]](#).
- [56] S. Chatrchyan *et al.* (CMS), *Eur. Phys. J. C* **72**, 1945 (2012), [arXiv:1202.2554 \[nucl-ex\]](#).
- [57] S. J. Brodsky and G. R. Farrar, *Phys. Rev. Lett.* **31**, 1153 (1973).
- [58] D. W. Sivers, S. J. Brodsky, and R. Blankenbecler, *Phys. Rept.* **23**, 1 (1976).
- [59] G. Aad *et al.* (ATLAS), *Eur. Phys. J. C* **73**, 2509 (2013), [arXiv:1304.4739 \[hep-ex\]](#).
- [60] D. Foreman-Mackey, D. W. Hogg, D. Lang, and J. Goodman, *Publ. Astron. Soc. Pac.* **125**, 306 (2013), [arXiv:1202.3665 \[astro-ph.IM\]](#).
- [61] M. Arneodo, *Phys. Rept.* **240**, 301 (1994).
- [62] K. J. Eskola, P. Paakkinen, H. Paukkunen, and C. A. Salgado, *Eur. Phys. J. C* **77**, 163 (2017), [arXiv:1612.05741 \[hep-ph\]](#).
- [63] R. Abdul Khalek, J. J. Ethier, J. Rojo, and G. van Weelden, *JHEP* **09**, 183 (2020), [arXiv:2006.14629 \[hep-ph\]](#).
- [64] P. Duventäster, L. A. Husová, T. Ježo, M. Klasen, K. Kovarič, A. Kusina, K. F. Muzakka, F. I. Olness, I. Schienbein, and J. Y. Yu, (2021), [arXiv:2105.09873 \[hep-ph\]](#).
- [65] H. Paukkunen, *PoS HardProbes2018*, 014 (2018), [arXiv:1811.01976 \[hep-ph\]](#).
- [66] J. Brewer, J. Thaler, and A. P. Turner, *Phys. Rev. C* **103**, L021901 (2021), [arXiv:2008.08596 \[hep-ph\]](#).

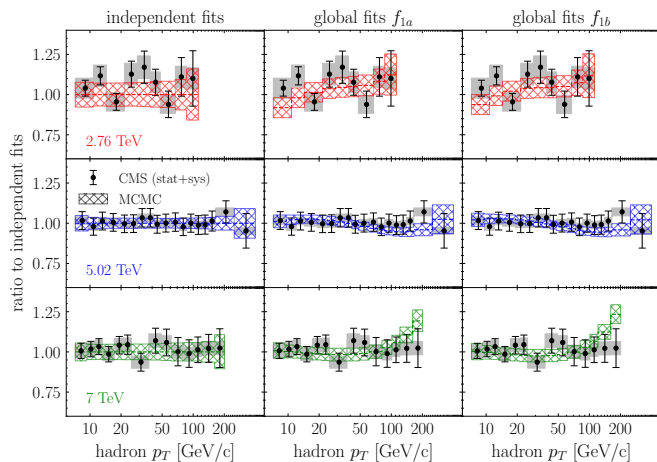


FIG. 10. Fits to CMS hadron spectra at $\sqrt{s} = 2.76, 5.02,$ and 7 TeV [7, 55, 56], anchoring the interpolation for the results for uncorrelated systematic uncertainties shown in Fig. 11. The left panel shows independent fits to the spectrum at each energy. The center and right panels show results for global fits f_{1a} and f_{1b} discussed in the main text. For visual clarity, all data and fits are normalized to the median value of the independent fit at that energy. Uncorrelated (statistical + systematic) uncertainties are shown in bars and luminosity uncertainties are grey boxes. Hatched bands indicate the 68% confidence interval of the MCMC fits.

[67] V. Khachatryan *et al.* (CMS), *Phys. Rev. Lett.* **105**, 022002 (2010), arXiv:1005.3299 [hep-ex].

Appendix A: MCMC fits to CMS hadron spectra

Here we perform MCMC global fits to CMS hadron data at $\sqrt{s} = 2.76, 5.02$ and 7 TeV. The measurements at 2.76 and 5.02 TeV are for $|\eta| < 1$ [7, 56] while at 7 TeV it is for $|\eta| < 2.5$ [55]. We apply a correction factor of 0.9705 to the 7 TeV spectrum that was obtained from the ratio of average multiplicity in $|\eta| < 1$ to $|\eta| < 2.5$ in the measured pseudorapidity distribution [67]. We use the inelastic hadronic cross-sections $61.8, 67.6,$ and 70.9 mb to convert $\sqrt{s} = 2.76, 5.02,$ and 7 TeV spectra to cross-sections [54]. Figure 10 shows fits to CMS hadron data with fully uncorrelated systematic uncertainties. We note that the dispersion in the data is large compared to the luminosity and statistical uncertainties only, and therefore assuming all systematic uncertainties to cancel gives high $\chi^2_\nu \approx 15.3$, indicating a poor fit quality. For that reason we show in Fig. 11 only results for fully uncorrelated systematic uncertainties ($\chi^2_\nu = 1.08$ and 1.13 for f_{1a} and f_{1b} respectively). We note that the interpolation using CMS data suggests a somewhat flatter p_T -dependence of the $6.37/5.02$ TeV ratio than comparable fits to the ALICE data from the main text (overlaid in grey), though they are consistent within large uncertainties.

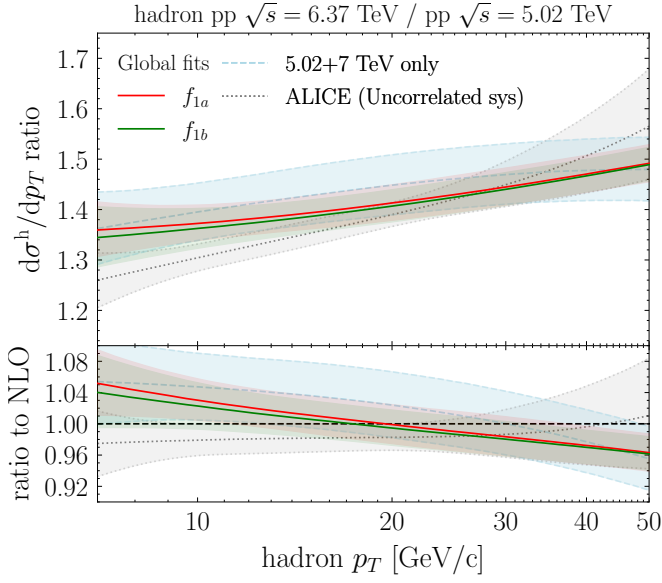


FIG. 11. Ratio of inclusive hadron spectra in pp collisions at 6.37 and 5.02 TeV (upper panel) and ratio to pQCD NLO (lower panel) for MCMC fits to CMS measurements. Bands show 68% confidence intervals around the median for f_{1a} (red) and f_{1b} (green) fit forms. Fits using only 5.02 and 7 TeV data are shown in light blue. Fits to ALICE hadron spectra using f_{1a} from Fig. 1c are shown in grey. In all curves systematic uncertainties are taken to be fully uncorrelated. Note the larger scale in the lower panel relative to the main text.